International Journal of Advanced Robotic Systems
January-February 2019: 1–8

DOI: 10.1177/1729881419826849
journals.sagepub.com/home/arx
SAGE

A dual-stage low-power converter driving for piezoelectric actuator applied in micro robot

Ye Mu, Tianli Hu, He Gong, Lijun Wang and Shijun Li

Abstract

In this article, a dual-stage converter driving for a piezoelectric actuator based on flyback circuit was designed and implemented, which could be applied in a micro robot. A low-voltage direct current could be converted to a high-voltage alternating current through flyback circuit and direct current/alternating current circuit in low-power condition. In the direct current/direct current stage, the charging and discharging process was realized to generate a high voltage bias from a low voltage directly supplied by battery. Then, the high voltage was converted into alternating waveform by an energy recovery circuit in direct current/alternating current stage. Experiments were conducted to verify the ability of the proposed converter to drive a 100-V-input piezoelectric bimorph actuator using a prototype 108 mg (excluding printed circuit board mass), 169 (13 × 13) mm^2, and 500-mW converter. According to the experimental results, this converter could be used for driving piezoelectric actuator applied in micro robot.

Keywords

Micro robot, piezoelectric actuator, high efficiency, small size, flyback converter

Date received: 30 October 2018; accepted: 6 January 2019

Topic: Mobile Robots and Multi-Robot Systems
Topic Editor: Quan Zhou
Associate Editor: Chen Chen

Introduction

Micro robot is a centimeter-scale robot with potential applications in searched-rescue, exploration, and reconnaissance.[1] An existing challenge of the research on micro robot is the sufficient power supply with high efficiency to implement kinds of actions, such as flying, crawling, and swimming.[2,3]

When the size of micro robot falls down to centimeter scale, the efficiency and power density of conventional actuators are significantly reduced because of the domination of surface effect.[4] To solve this limitation, piezoelectric actuators that work as an alternative solution were paid more attention.[5] Meanwhile, Wood et al. considered a complete fabrication solution for actuators, links, flexures, integrated wiring, and structural elements using high-performance materials.[6] They then developed a highly efficient transmission link for a specific device.

Meanwhile, the matching voltage conversion circuits should be designed to satisfy the electrical requirements of piezoelectric actuators.[7] Several researchers have discussed the miniaturization of voltage conversion circuits for microrobotic applications. A boost converter cascaded with a switched capacitor circuit was adopted by Steltz et al. to obtain high voltage.[8] However, this structure requires a large number of pump capacitors, which increases the size of the circuit and reduces its power density, particularly at a high output power. Other topologies

College of Information Technology, Jilin Agricultural University, Changchun, China

Corresponding author:
Ye Mu, College of Information Technology, Jilin Agricultural University, 2888 Xincheng Street, Changchun, Jilin 130018, China.
Email: muye@jlau.edu.cn

with more components and a high step-up ratio are also suitable for driving high-voltage reactive loads; however, most efforts have focused on large-scale and high-power applications.[9–11] In another part of the circuit, a simple push–pull driver described in the study by Steltz et al.[8] can generate a unipolar square wave voltage across the load without energy recovery. The majority of the existing topologies focus on efficient piezoelectric driving for large-scale and high-power applications, which reduces the efficiency and power density of the power supply.[12–17] Harvard's team has previously produced a small-scale power conversion interface. However, as described in the study by Karpelson et al.,[18] the boost tapped-inductors they use have difficulty in manufacturing compared to general flyback transformers. At the same time, in the direct current (DC)–alternating current (AC) stage, the detection of current becomes quite difficult in the case of low power. This article is dedicated to improving and validating the short board mentioned above.

In this article, a dual-stage low-power converter driving for piezoelectric actuator was designed and implemented. A low voltage coming from battery was converted into 150-V high alternating voltage which is capable of driving the piezoelectric actuator. In addition, this manuscript presents (a) the requirements and strategies of driving piezoelectric actuator, (b) the working principle and control scheme of the dual-stage low-power converter, including DC/DC flyback conversion stage and DC/AC driving stage, (c) the experimental validation adopts converter prototype driving for piezoelectric actuator, and (d) the conclusions and future prospects.

Requirements and strategies driving for piezoelectric actuator

In terms of piezoelectric actuators, the size of displacement is proportional to the excitation voltages within the endurable voltage range. In most applications, to supply a desired high voltage, an external bulky power supply is the common choice which inevitably limits the size reduction. Therefore, a compact converter with high step-up ratio driving for piezoelectric actuator is desired.

Prior work about driving methods of piezoelectric actuator includes efforts by Rios and Fleming,[19] which made the detailed analysis of the efficiency of several different configurations.[20] The common driving method to drive piezoelectric bimorph is named as "simultaneous drive," as shown in Figure 1.

In "simultaneous drive" mode, a DC bias boost stage is connected to the two compliant electrodes, whereas a suitable unipolar drive stage is applied to the central compliant elastomer film. The simultaneous driving architecture exhibits the advantage of using fewer components to reduce the size and mass of the converter when multiple bimorphs are required in a system.[20] When the AC voltage is operating in the positive half cycle, the upper layer of the bimorph produces less contraction than the bottom layer, which causes the bending actuator to exhibit downward displacement.[21]

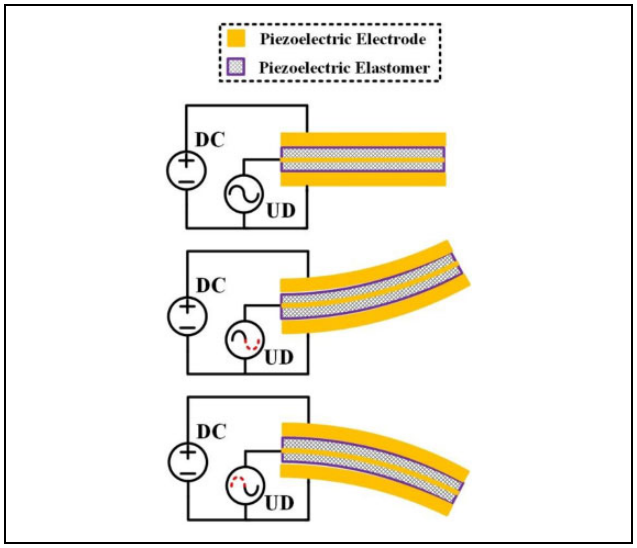

Figure 1. Drive methods for piezoelectric actuator.

Driving converter design

The converter shown in Figure 2 was designed as dual-stage circuit.[8,22] The first stage was DC/DC circuit using flyback converter which realized the boosting from a low-voltage DC to a high-voltage DC. The second stage is DC/AC converter circuit using bidirectional active half bridge which efficiently recycled unused energy.

DC/DC conversion stage

Compared with other forward topologies, the advantage of the flyback converter is that the output filter inductor is not necessary, which reduces the size of the converter.[9] A flyback converter is shown in Figure 3.

The operation of flyback converter can be divided into discontinuous current mode (DCM) and continuous current mode. Considering the requirement of high step-up ratio, the flyback converter should be working in DCM. An ideal switching waveforms of the adopted flyback converter operating in DCM are shown in Figure 4.

When the switch Q is turned on, the current i_{L1} through the magnetizing inductor L_1 goes up. When the switch Q is turned off, the magnetic energy stored in L_1 is transferred to the secondary side. In the charging and discharging period, the diode current i_{L2} decreases from an initial value to zero at the end of this period. Furthermore, the diode D is designed to prevent the reverse current from i_{L2} which would remain i_{L2} to zero during the discharging period. In DCM, the voltage step-up ratio is written as

$$\frac{V_c}{V_{bat}} = D \cdot n \cdot \sqrt{\frac{R}{2L_1 f_s}} \quad (1)$$

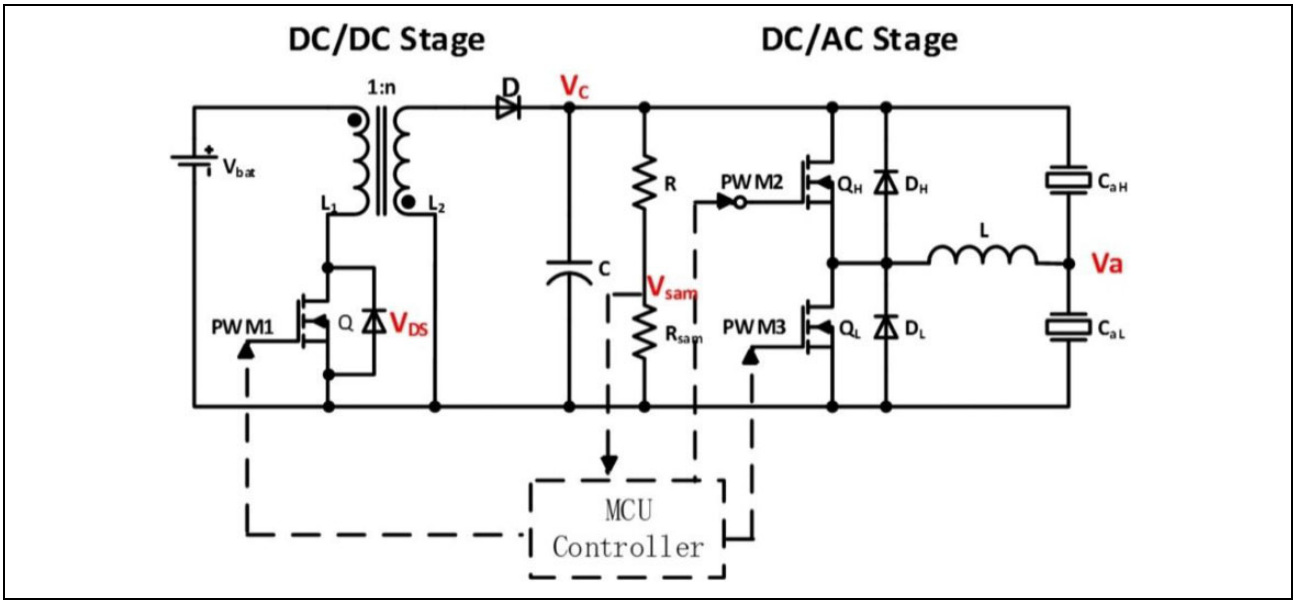

Figure 2. Dual-stage converter.

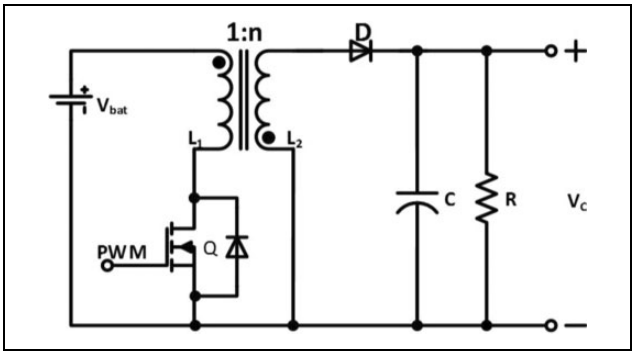

Figure 3. Flyback circuit.

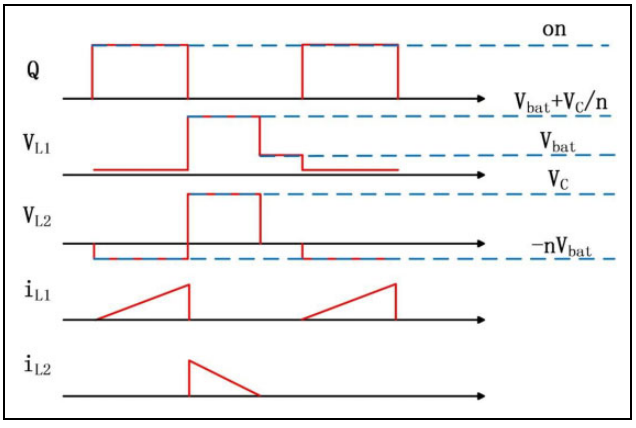

Figure 4. Switching waveforms of the adopted flyback working in DCM. DCM: discontinuous current mode.

where V_{bat} is the output voltage of lithium battery, V_c denotes the output voltage, D represents the controllable duty cycle, n is the turns ratio of transformer, R is the equivalent resistance of load, L_1 is the primary inductance of transformer, and f_s is the switching frequency.

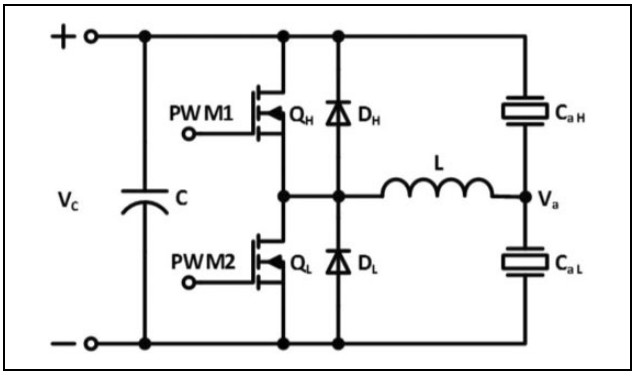

Figure 5. DC/AC converter. DC: direct current; AC: alternating current.

DC/AC drive stage

To improve the conversion efficiency, the DC/AC drive stage should be able to recover unused energy from capacitive load.[23] In the existing optional methods to generate the arbitrary drive signal, the switching half-bridge has the desired compact structure. Nevertheless, only the square wave is able to be generated without unused energy recovery.[11] For another option, a pulse width modulation output was generated by a switching half-bridge and filtered by an RC network to produce an arbitrary output waveform. In this case, high losses are invertible due to the dissipation of a large amount of energy from the resistor.

A DC/AC drive stage is shown in Figure 5, which can realize energy transfer between two capacitive loads. When energy is delivered to the load, this circuit works in a step-

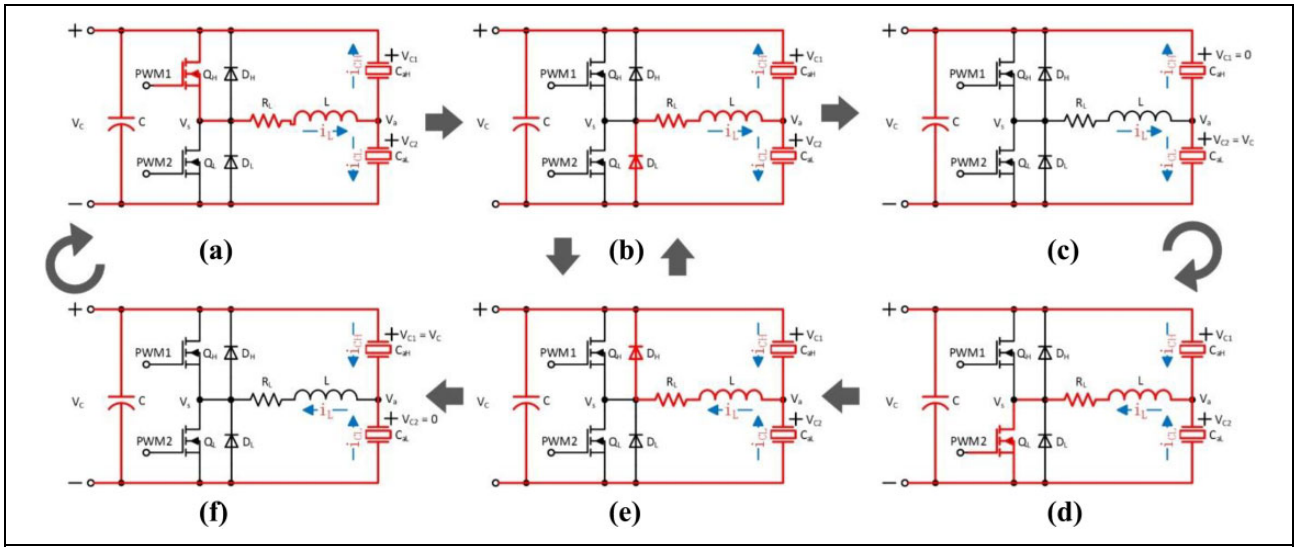

Figure 6. Energy transformation in the high-voltage drive stage.

down mode. By contrast, when energy is removed from the load, it works in a step-up mode. Inductor and the intrinsic actuator capacitance, this design is able to both generate an arbitrary unipolar output waveform and recover unused energy from the load.

When the high-side switch Q_H is turned on, the current through the inductor begins to rise. When Q_H is turned off, the inertia current charges the node V_a through the diode D_L. By contrast, the energy stored in node V_a is released to the capacitor V_c while low-side switch Q_L is turned on. And then, residual current continues to discharge through the diode D_H when Q_L is turned off. The output waveform can be generated at V_a by generating the sequence of charge and discharge pulses at the appropriate time. Only a small amount of energy is lost during the transformation in each switching period, which enhances the conversion efficacy.

DC/AC energy transform

In the proposed converter, the energy transform can be divided into two parts. The first part occurs in the flyback converter operating in DCM. When the switch is turned on, the energy stored in the capacitor provides the DC/AC converter. When the switch is turned off, the transformer supplies energy to the capacitor as compensation. The second part exists in DC/AC drive stage. A waveform cycle can be divided into six modes which was used to illustrate the energy transform, as shown in Figure 6.

In mode (a), when switch Q_H is turned on, inductor current i_L is increased. Unused energy in the electrostatic actuator at upper side is transferred to lower side. According to Kirchhoff's law, we can get

$$L \cdot \frac{\partial i_L}{\partial t} + R_L \cdot i_L + V_{C2} = V_C \tag{2}$$

Table 1. The parameters used in formula.

Parameter	Value
Neper frequency β	$\frac{R_L}{2L}$
Angular resonance frequency ω_0	$\frac{1}{\sqrt{2LC_2}}$
ecaying oscillation frequency ω_d	$\sqrt{\omega_0^2 - \beta^2}$

$$C_2 \cdot \frac{\partial V_{C2}}{\partial t} = i_{C2} = i_L + i_{C1} = i_L + C_1 \cdot \frac{\partial V_{C1}}{\partial t} \tag{3}$$

As a result, the calculated formula could be expressed as

$$\frac{\partial^2 V_{C2}}{\partial t^2} + 2\beta \cdot \frac{\partial V_{C2}}{\partial t} + \omega_0^2 \cdot V_{C2} = \omega_0^2 \cdot V_C \tag{4}$$

Under the underdamped oscillation condition $(\beta^2 - \omega^2 < 0)$

$$V_{C2}(t) = V_C - V_C \cdot e^{-\beta t}\left(\cos \omega_d t + \frac{\beta}{\omega_d} \sin \omega_d t\right) \tag{5}$$

where the used parameters are listed in Table 1.

Table 1 represents the parameters used in formula.

According to the theoretical calculation, the drive signal voltage V_{C2} increases approximately to V_C.

In mode (b), when Q_H is turned off, the inductor current i_L is decreased and flows through the freewheeling diode D_L

$$L \cdot \frac{\partial i_L}{\partial t} + R_L \cdot i_L + V_{C2} = 0 \tag{6}$$

$$C_2 \cdot \frac{\partial V_{C2}}{\partial t} = i_{C2} = i_L + i_{C1} = i_L + C_1 \cdot \frac{\partial V_{C1}}{\partial t} \tag{7}$$

As a result, the calculated formula could be expressed as

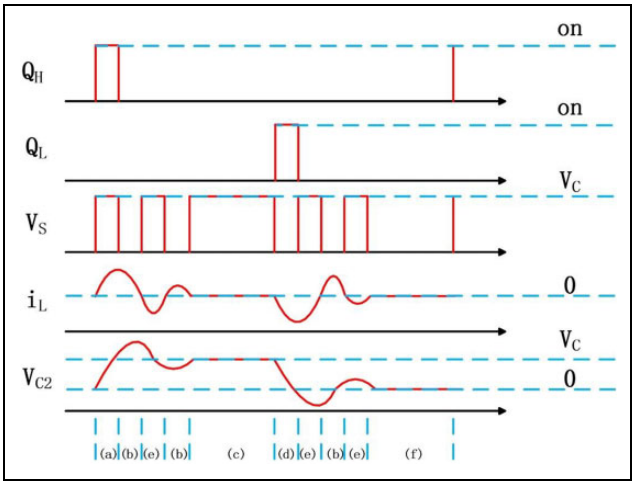

Figure 7. Waveform in an energy transfer cycle.

$$V_{C2}(t) = V_C \cdot e^{-\beta t}\left(\cos\omega_d t + \frac{\beta}{\omega_d}\sin\omega_d t\right) \quad (8)$$

The drive signal voltage $V_{C2}(t)$ decreases while the energy stored in the inductor L is begin to release.

In mode (c), the electrostatic actuator at the lower side is fully charged while the electrostatic actuator at the upper side and inductor L are exhausted. In this period, the drive signal voltage V_{C2} is the same with V_C. The whole unused energy of actuator is transferred from the upper side to the lower side.

In mode (d), when switch Q_L is turned on, inductor current i_L increases in reverse. Unused energy of piezoelectric actuator at the lower side is transferred to the inductor L.

$$V_{C2}(t) = V_C \cdot e^{-\beta t}\left(\cos\omega_d t + \frac{\beta}{\omega_d}\sin\omega_d t\right) \quad (9)$$

In mode (e), when switch Q_L is turned off, inductor current i_L is decreased and flows through the freewheeling diode D_L. Energy is transferred to the piezoelectric actuator at the upper side

$$V_{C2}(t) = V_C - V_C \cdot e^{-\beta t}\left(\cos\omega_d t + \frac{\beta}{\omega_d}\sin\omega_d t\right) \quad (10)$$

In mode (f), the drive signal voltage $V_{C1}(t)$ is charged same as V_C while unused energy of piezoelectric actuator is completely transferred from the lower side to the upper side.

The mentioned energy transfer cycle is shown in Figure 7, two drive signals with a phase difference of 180° can be generated to drive the piezoelectric actuator by controlling the charge and discharge period.

To achieve high conversion efficiency, the unused energy in capacitive piezoelectric actuator is used, and the overall efficiency of the system is enhanced effectively.

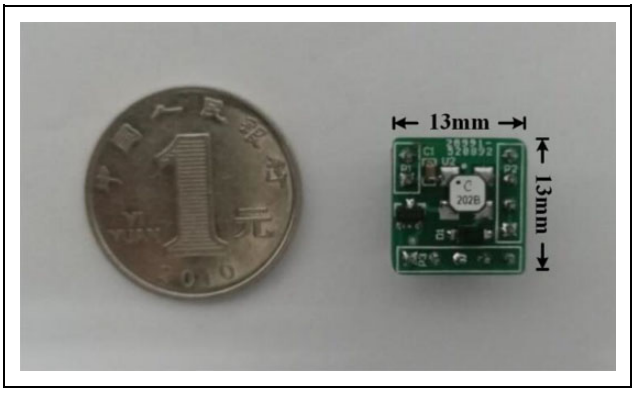

Figure 8. Image of the converter prototpye.

Table 2. Specifications of the discrete components.

	Chip number	Weight (mg)	Size (mm)
Flyback transformer	LPR4012	64	4 × 4
Power MOSFET (power stage)	SI2304	8	2.8304M
Rectifier diode	SMD1200PL	8	2.81200
Capacitor (power stage)	1 μF/200 V	1.2	1.6F/20
Power MOSFET (drive stage)	TN2404K	8	2.8404K
Inductor (drive stage)	15 μH/40 mA	1.2	1.6 × 0.8

Experimental results

Based on the mentioned theory, a converter prototype used for driving piezoelectric actuators was realized.

The prototype of converter

The circuit topology described in Figure 8 is soldered onto a well-designed printed circuit board using discrete components. Table 2 lists the specifications of the discrete components, which include a power MOSFET, a rectifier diode, a flyback transformer, and a filtering capacitor. The flyback step-up stage is responsible for increasing the input DC voltage. The basis of the selection is to ensure that the components can handle the predicted voltage and current without breakdown and failure.

Table 2 provides the specifications of the discrete components.

Using the abovementioned components, a prototype weighing 108 mg was fabricated. The length, width, and thickness of the circuit are 13, 13, and 4 mm, respectively. The image of the fabricated converter is shown in Figure 8.

Circuit experimental analyses

A low-voltage source lithium battery is utilized to generate high drive voltage in the developed topology. The input voltage of the dual-stage drive circuit is 3.7 V, and the

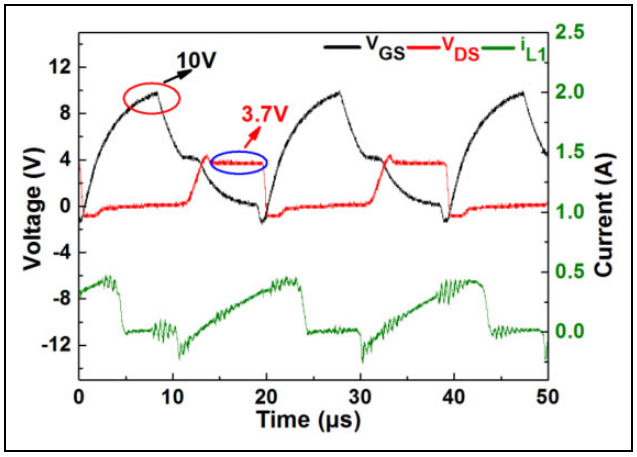

Figure 9. Nodes waveforms of the flyback converter.

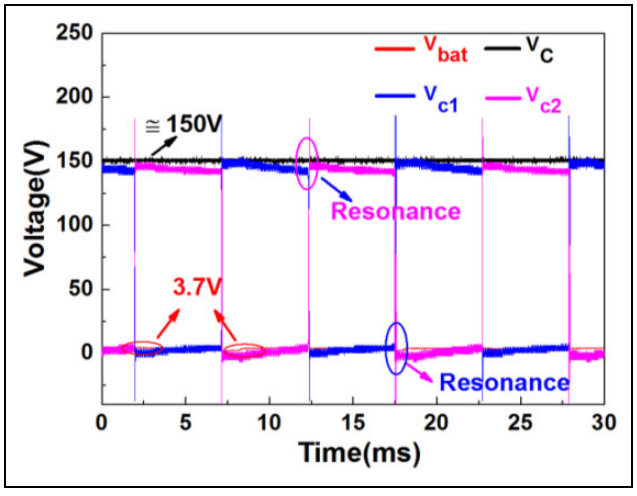

Figure 10. Output voltage waveforms of the DC/DC flyback converter and the DC/AC driving stage. DC: direct current; AC: alternating current.

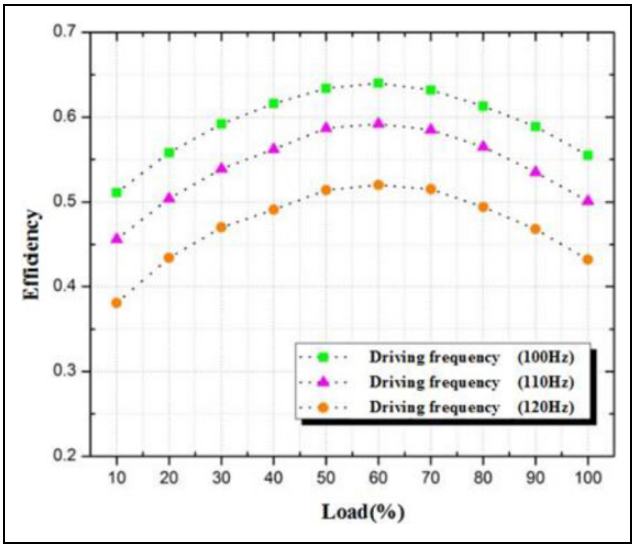

Figure 11. Efficiency vs. load for the three different driving frequencies.

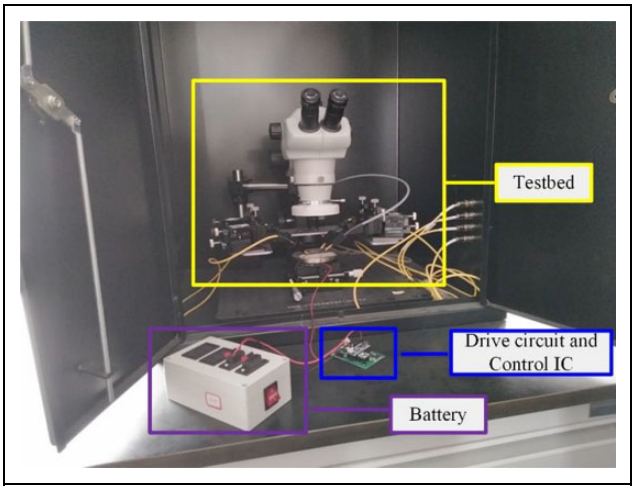

Figure 12. Image of the entire system.

output voltage is regulated at 150 V. The experimental results are shown in Figures 9 to 11.

As shown in Figure 9, nodes waveforms of V_{GS}, V_{DS}, and i_{L1} were obtained. The waveforms are consistent with the theoretical analysis. The zero current shows that the circuit worked in flyback DCM.

For the switch to be fully operated, the drive voltage to control switch Q is high to 10 V. When the switch Q is turned on, the voltage V_{DS} crosses switch Q and immediately reduces down to zero, and the current i_{L1} is increased linear to store energy. When the switch Q is turned off, the voltage is maintained equal to the lithium battery voltage of 3.7 V, and the energy stored in the primary side in previous cycle transfers to the secondary side. At this time, the current goes down to zero, which shows that flyback converter is working in DCM.

In DC/AC drive stage, a regulated time-variable voltage with 150 V and the two alternative driving voltages are shown in Figure 10, which meets the driving requirement of piezoelectric bimorph actuator.

In DC/DC flyback stage, a regulated high-voltage DC of 150 V is generated from the lithium battery voltage 3.7 V. The high step-up ratio is high up to almost 41 times. Two 180° out-of-phase square drive signals, with amplitude of approximate 150 V and frequency of 100 Hz, are achieved at the drive stage. LC resonance between the inductor L and two nanocapacitors occurs at the beginning of each half-switching cycle. Small inductance is required to increase the resonance frequency, which further decreases the overshoot of the square drive signal.

Figure 11 demonstrates the efficiency of the proposed interface in terms of various loads and drive signal frequencies.

The loads continuously increase from 10% to 100% with 10% intervals. The three driving frequencies are 100, 110,

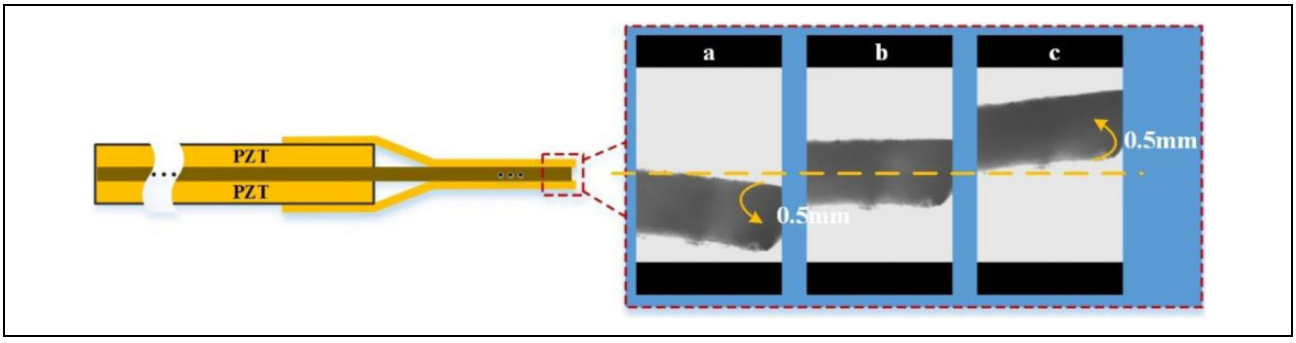

Figure 13. Image of the piezoelectric actuator displacement: (a) down, (b) at equilibrium, and (c) up.

and 120 Hz. The peak efficiency (64.5%) can be reached at 60% load and 100 Hz driving frequency, which is higher than the maximum conversion efficiency of 42.4% obtained in the study by Kovacs et al.[20]

PZT driving validation

The piezoelectric bimorph ceramic material (QDTE52-7.0-0.82-4, PANT, Suzhou, China) used to test dynamic performance has the following parameters: 190 V highest driving voltage, 52 mm long, 7 mm wide, 0.82 mm thick, and 1.2 mm bidirectional displacement. The first resonant frequency of each bimorph layer is approximately 100 Hz close to the driving frequency of an insect-type robot, which makes the research practical.

Figure 12 shows the image of the entire system, which comprises a battery box, the proposed drive circuit, and a manual probe station that is used in conjunction with a B1505A I/V Agilent power device analyzer. The output of the drive circuit is connected to the terminal of the probe, and the piezoelectric actuator is physically anchored by the terminal under the electron microscope.

Similarly, the bidirectional displacements shown in Figure 13 are achieved with −100, 0, and 100 V excitation generated by the proposed circuit, which illustrate the piezoelectric bimorph at down (Figure 13), equilibrium (Figure 13(b), and up (Figure 13(c), respectively. The experimental results show that the mechanical displacement is proportional to the square of the driving voltage. The displacement of the up–down motion is close to 1 mm, which can be further expanded by mechanically magnifying the structure to obtain potential applications in micro robot application.

Conclusions and prospects

The designed converter driving for a piezoelectric bimorph is implemented, which can be applied in micro robot application. In DC/DC conversion stage, flyback converter working in DCM was used to boost the voltage with high step-up ratio. In DC/AC drive stage, the recycling energy from capacitive load (piezoelectric actuator) enhances efficiency of the overall circuit. The micro-displacement of piezoelectric bimorph actuator is validated using alternative high drive voltage. Our next work will include further reduction in circuit losses to improve efficiency and a chip-based design to reduce size and mass, with further development in the miniaturization of the electronic component.

Declaration of conflicting interests

The author(s) declared no potential conflicts of interest with respect to the research, authorship, and/or publication of this article.

Funding

The author(s) disclosed receipt of the following financial support for the research, authorship, and/or publication of this article: This research was supported by the Science and Technology Department of Jilin Province, China (nos 20160623016TC, 20170204017NY, 20170204038NY, and 20180201022GX), the College Students Innovation and Entrepreneurship Training Program of Jilin Province, China (nos 2017490 and 2017493), and the Education Department of Jilin Province of China (no. JJKH20180154KJ).

ORCID iD

Ye Mu https://orcid.org/0000-0002-4599-0293

References

1. Ceylan H, Giltinan J, Kozielski K, et al. Mobile microrobots for bioengineering applications. *Lab Chip* 2017; 17(10): 1705–1724.
2. Gregory J, Fink J, Stump E, et al. *Application of Multi-Robot Systems to Disaster-Relief Scenarios with Limited Communication. Field and Service Robotics*. Springer International Publishing, 2016.
3. Li L and Wu Z. Research on automatic navigation of unmanned aerial vehicle based on 3D laser scanning. *Laser J* 2018; 39: 91–95.
4. Lv X, Wei WW, Mao XU, et al. A novel mems electromagnetic actuator with large displacement. *Sensors Actuators A Phys* 2015; 221: 22–28.
5. Mineta T, Mitsui T, Watanabe Y, et al. An active guide wire with shape memory alloy bending actuator fabricated by room temperature process. *Sensors Actuators A Phys*. 2001; 97(4): 632–637.

6. Wood RJ, Avadhanula S, Sahai R, et al. Microrobot design using fiber reinforced composites. *J Mech Design* 2008; 130(5): 680–682.
7. Towfighian S, Seleim A, Abdelrahman EM, et al. A large-stroke electrostatic micro-actuator. *J Micromech Microeng* 2011; 21(7): 075023.
8. Steltz E, Seeman M, and Avadhanula S. Power electronics design choice for piezoelectric micro robots. In: *2006 IEEE/RSJ International Conference on Intelligent Robots and Systems*, Beijing, China, 9–15 October. 2006, 1322–1328, IEEE.
9. Luo FL and Ye H. Positive output cascade boost converters. *Proc IEEE Electric Power Appl* 2004; 151(5): 590–606.
10. Chen SM, Yang LS, Chen JF, et al. A single switch boost-flyback dc-dc converter integrated with switched-capacitor cell. In: *Proc IEEE 8th International Conference on Power Electronics and Ecce Asia*, Jeju, Korea, 30 May-3 June 2011, 2782–2787. IEEE.
11. Liao WC, Liang TJ, Liang HH, et al. Study and implementation of a novel bidirectional dc-dc converter with high conversion ratio. In: *Proc IEEE Energy Conversion Congress and Exposition*, Phoenix, Arizona, USA, 17–22 September 2011, 134–140. IEEE.
12. Campolo D, Sitti M, and Fearing RS. Efficient charge recovery method for driving piezoelectric actuators with quasi-square waves. *IEEE Trans Ultrasonics Ferroelectrics Frequency Control* 2003; 50(3): 237–244.
13. Li X. Laser power beaming for UAVs. *Laser J*. 2013; 34: 18–19.
14. Zsurzsan GT, Zhang Z, Andersen MMA, et al. Class-D amplifier design and performance for driving a piezo actuator drive servomotor. In: *IEEE International Conference on Industrial Technology*, Taipei, Taiwan, 14–17 March 2016, 1068–1072. IEEE.
15. Liu F, Lin J, and Wang Y. The design of high precision QCL driver for micro laser impulsed unmanned aerial vehicle. *Laser J* 2014; 35: 75–77.
16. Luan J. *Design and Development of High-Frequency Switching Amplifiers Used for Smart Material Actuators With Current-Mode Control*, Master's Thesis, Virginia State University, USA, 1998.
17. Li Q, Hao X, He J, et al. The influences of refractive index sensing of metamaterials with different size of dielectric layer. *Laser J* 2016; 37: 14–17.
18. Karpelson M, Whitney JP, Wei G, et al. Design and fabrication of ultralight high-voltage power circuits for flapping-wing robotic insects. In: *2011 Twenty-Sixth Annual IEEE Applied Power Electronics Conference and Exposition (APEC)*, Fort Worth, TX, USA, 6–11 March 2011, 2070–2077, IEEE.
19. Rios SA and Fleming AJ. A new electrical configuration for improving the range of piezoelectric bimorph benders. *Sensors Actuators A Phys* 2015; 224: 106–110.
20. Kovacs G, Düring L, and Michel S. Stacked dielectric elastomer actuator for tensile force transmission. *Sensors Actuators A Phys* 2009; 155(2): 299–307.
21. Karpelson M, Wei GY, and Wood RJ. Driving high voltage piezoelectric actuators in microrobotic applications. *Sensors Actuators A Phys* 2012; 176(4): 78–89.
22. Chen C, Liu M, Lin J, et al. Piezoelectric transformer-based high conversion ratio interface for driving dielectric actuator in microrobotic applications. *Int J Adv Robot Syst* 2016; 13(5): 1729881416657957. DOI: 10.1177/1729881416657957.
23. Liang TJ, Chen SM, Yang LS, et al. A single switch boost-flyback DC-DC converter integrated with switched-capacitor cell. In: *8th International Conference on Power Electronics - ECCE Asia*, Jeju, South Korea, 30 May–3 June 2011 (pp. 2782–2787). IEEE.